Sugar beet cold-induced PMT5a and STP13 carriers are poised for taproot proton-driven plasma membrane sucrose and glucose import

Antonella Reyer, Nadia Bazihizina, Sönke Scherzer, Justyna Jaślan, Nadine Schäfer, Dawid Jaślan, Tracey Ann Cuin, Khaled a S Al-Rasheid, Ahmed H Alfarhan, Saleh A Alquraishy, et al.

Sugar beet cold-induced PMT5a and STP13 carriers are poised for taproot proton-driven plasma membrane sucrose and glucose import

Antonella Reyer[1], Nadia Bazihizina[1,2], Sönke Scherzer[1], Justyna Jaślan[1,3], Nadine Schäfer[1], Dawid Jaślan[1,4], Tracey Ann Cuin[1,5], Khaled A.S. Al-Rasheid[6], Ahmed H. Alfarhan[6], Saleh A. Alquraishy[6], Frank Ludewig[7], Wolfgang Koch[7], Karsten Harms[8], Dirk Becker[1], Thomas D. Mueller[1], Benjamin Pommerrenig[9], H. Ekkehard Neuhaus[9], Irene Marten[1], Rainer Hedrich[1*]

[1] Molecular Plant Physiology and Biophysics, University of Würzburg, 97082 Würzburg, Germany

[2] Department of Agrifood Production and Environmental Sciences, Università degli Studi di Firenze, Viale delle Idee 30, 50019 Sesto Fiorentino, Florence, Italy

[3] BPMP, Univ Montpellier, CNRS, INRAE, Institut Agro, Montpellier, France

[4] Walther Straub Institute of Pharmacology and Toxicology, Faculty of Medicine, Ludwig Maximilians-Universität, 80336 Munich, Germany

[5] Biological Sciences, School of Natural Sciences, University of Tasmania, Hobart, TAS, 7005 Australia

[6] College of Science, King Saud University, 11451 Riyadh, Saudi Arabia

[7] KWS SAAT SE, Einbeck, Germany

[8] Südzucker AG, Central Department for Research, Development, and Service, 67283 Obrigheim/Pfalz, Germany

[9] Plant Physiology, University of Kaiserslautern, 67663 Kaiserslautern, Germany

*Author for correspondence: Rainer Hedrich (hedrich@botanik.uni-wuerzburg.de)

Summary

- As the major sugar-producing crop in the northern hemisphere, sugar beet taproots store sucrose at a concentration of about 20 %. While the vacuolar sucrose loader TST has already been identified in the taproot, sugar transporters mediating sucrose uptake across the plasma membrane of taproot parenchyma cells remained unknown.
- We electrophysiologically examined taproots for proton-coupled sugar uptake and identified potentially involved transporters by transcriptomic profiling. After cloning, the transporter features were studied in the heterologous *Xenopus laevis* oocyte expression system using the two-electrode voltage clamp technique. Insights into the structure were gained by 3D homology modeling.
- As with glucose, sucrose stimulation of taproot parenchyma cells caused inward H^+-fluxes and plasma membrane depolarization, indicating a sugar/proton symport mechanism. As one potential candidate for sugar uploading, the BvPMT5a was characterized as a H^+-driven low-affinity glucose transporter, which does not transport sucrose. BvSTP13 operated as a high-affinity H^+/sugar symporter, transporting glucose and to some extent sucrose due to a binding cleft plasticity. Both transporter genes were upregulated upon cold exposure, with the transport capacity of BvSTP13 being more cold-resistant than BvPMT5a.
- Identification of BvPMT5a and BvSTP13 as taproot sugar transporters could improve breeding of cold-tolerant sugar beet to provide a sustainable energy crop.

Key words: cold, glucose, plasma membrane transport, PMT5a, proton-driven sugar transport, STP13, sucrose, sugar beet (*Beta vulgaris*)

Introduction

Sugar beet (*Beta vulgaris*) and sugarcane (*Saccharum officinarum*) together account for the world's sugar production. Industrial production of sugar from the sugar beet taproot began in the early nineteenth century and since then, breeding has increased the sugar content from 8% to about 21 %. From the late 1970s to the present, plant scientists have been trying to identify the transport proteins that translocate sucrose from the sugar factories in the leaf to its final depot in the taproot. In the early days of sugar beet (*Beta vulgaris*) research, sucrose transport was examined in taproots, leaf discs and plasma membrane-enriched vesicles (Wyse, 1979; Bush, 1989; Sakr *et al.*, 1993). Translocation of sucrose against its concentration gradient requires metabolic energy. The first *in vitro* evidence for a proton-driven sucrose symport, which uses the proton motive force (PMF) as a secondary energy source for solute uphill transport, was provided by Bush (1989). Sucrose import was also found very sensitive to changes in electrical membrane potential as well as to orthovanadate, an inhibitor of the H^+-ATPase, whose H^+ pumping ability is required to keep the resting membrane voltage hyperpolarized, and to retain the inward H^+ gradient (Buckhout, 1989; Bush, 1990; Michonneau *et al.*, 2004).

With the beginning of the molecular era, the nature of the first plant glucose and sucrose transporters were identified (Sauer & Tanner, 1989; Sauer *et al.*, 1990; Riesmeier *et al.*, 1992). In 2013, the genome of *Beta vulgaris* was sequenced (Dohm *et al.*, 2014), providing molecular access to the transporter inventory of sugar beet. Among them, BvSUT1 was demonstrated to represent a proton-driven transporter sucrose loader of the sugar beet phloem in source leaves (Nieberl *et al.*, 2017), while the BvTST2.1 transporter was shown to be responsible for vacuolar sucrose accumulation in the sugar beet taproots (Jung *et al.*, 2015). In patch-clamp studies with vacuoles of BvTST2.1-overexpressing tobacco mesophyll cells, this sucrose-specific transporter was characterized as a proton/sucrose antiporter, which couples the import of sucrose into the vacuole with the export of protons (Jung *et al.*, 2015) Release of vacuolar sucrose and glucose is mediated by sugar symporters of the BvSUT4/AtSUC4 and BvIMP/AtERDL6 types (Schulz *et al.*, 2011; Schneider *et al.*, 2012; Klemens *et al.*, 2014; Rodrigues, C. M. *et al.*, 2020).

Despite recent advances in *in vitro* culture and genetic transformation technologies incorporated with classical sugar beet breeding programs, it takes about 4 - 5 years to generate transgenic sugar beet plants. Low regeneration and transformation frequencies still oppose serious restrictions for routine application of transformation technologies (Gurel *et al.*, 2008). Thus, after almost 40 years of research our current knowledge about sugar transport in *Beta*

vulgaris is essentially that of the 1980's (Wyse, 1979; Saftner & Wyse, 1980; Saftner *et al.*, 1983; Lemoine *et al.*, 1988; Fieuw & Willenbrink, 1990) and is restricted to leaf phloem loading and taproots' vacuolar transport. The molecular identity and the functional properties of transporters that provide for sugar uptake into the taproot storage parenchyma cells is unknown.

Plants respond to cold temperatures by accumulating compatible solutes (e.g., proline, polyols, soluble sugars such as sucrose, glucose and fructose) to protect cellular integrity (Wanner & Junttila, 1999; Gusta *et al.*, 2004; Krasensky & Jonak, 2012; Klemens *et al.*, 2014; Tarkowski & Van den Ende, 2015). Interestingly, altered vacuolar glucose levels are accompanied by changes in vacuolar sugar transporter gene activities. In Arabidopsis plants, a lower transcript level of the vacuolar glucose unloader AtERDL6 alongside a higher level of the vacuolar glucose loader AtTST1/2 was detected upon cold exposure (Poschet *et al.*, 2011). Further results from studies with AtTST1 loss-of-function and BvIMP-overexpressing Arabidopsis plants suggested that the ability of the plant to accumulate monosaccharides in vacuoles under cold conditions accounts for frost tolerance (Klemens *et al.*, 2014). In comparison, in cold-treated sugar beet taproots, the transcription of the vacuolar sucrose loader BvTST2.1, which is a homolog to AtTST1/2, was down-regulated, whereas that of the vacuolar sucrose unloader BvSUT4 increased (Rodrigues, Cristina Martins *et al.*, 2020), a finding that may be related to the cold sensitivity of the sugar beet plant.

To elucidate the nature of sucrose and glucose transport function in taproot of sugar beet, in this study, we employed *in vivo* voltage-recording and proton-sensing microelectrodes to monitor sucrose- and glucose-dependent changes in the membrane voltage and H^+ flux in taproot slices directly. To identify the molecular players, we conducted comprehensive phylogenetic and transcriptomic analysis of the sugar beet monosaccharide transporter (MST) family proteins and sugar beet taproot tissue during low temperatures. We identified the taproot expressed BvPMT5a and BvSTP13, both are up-regulated upon exposure to cold temperatures. Thorough electrophysiological characterization using *Xenopus laevis* oocytes as a functional expression system together with molecular modelling identified both carriers as the long-sought proton-driven transporters sugar exhibiting distinct substrate specificities. Based on these results, we conclude that both BvPMT5a and BvSTP13 are well suited to mediate differential glucose and sucrose uptake across the taproot plasma membrane and discuss their possible physiological role during sugar beet cold stress adaptation.

Materials and Methods

Plant material and cultivation

For electrophysiological characterization and RT-qPCR analysis, *Beta vulgaris* plants (GT1-3 hybrids, Lisanna) derived from KWS SAAT SE (Germany) were cultivated on Profi Substrat soil (CL ED73 Puls + Eisen, Einheitserde Werkverband e.V) under a 14/10 h day/night regime with a light intensity of about 120 µmol m^{-2} s^{-1} (sodium vapor lamp Sonte Agro 400) The temperature was 24 °C and the relative humidity 60%.

Membrane voltage recordings in sugar beet taproots

Plants of 95 to 115 days old were used for membrane voltage recordings. The taproots were harvested, and cross sections of whole root prepared (middle part of the root, 0.5 mm slice). From these slices, the periderm was detached with sharp forceps to create a window. The tissue in this window was cut tangential to get a sample of 10 to 15 cell layers thick. The sample was glued with medical adhesive B liquid (ULRICH Swiss, St Gallen, Switzerland) to a cover glass, which was mounted with double-sided adhesive tape in the lid of a 3 cm Petri dish. It was bathed in 3 mL measuring solution (1 mM $CaCl_2$, 1 mM KCl, 10 mM 2-(N-morpholino)ethanesulfonic acid (MES), adjusted with Bis-Tris propane (BTP) to pH 6.0) and the sample was incubated for 16 h at 18 °C in the dark. The solution was changed 1 h before measurement, and samples remained in the dark. The free-running membrane voltage recordings were essentially performed as described (Reyer *et al.*, 2020). Briefly, glass microelectrodes made of borosilicate glass capillaries (length 100 mm, $Ø_{outer}$ 1.0 mm, wall thickness 0.21 mm, Hilgenberg GmbH, Malsfeld, Germany) and filled with 300 mM KCl were impaled into the cells under microscopic control. The acquired data were analyzed using Microsoft Excel 2010 and Origin Pro-2021.

Proton flux measurements on sugar beet taproots

For application of the scanning ion-selective electrode (SISE) technique (Dindas *et al.*, 2018), taproots were cut into slices (Ø ~ approx. 0.5 cm) and an intact layer of parenchyma cells was dissected from a small area of such a slice. The entire slices were then immediately incubated in a basic salt medium (BSM, 0.5 mM KCl; 0.1 mM CaCl, pH 5.3 unbuffered) and left overnight in the dark at room temperature. One hour prior to measurement, the slices were mounted with non-woven microporous adhesive tape (URGOPORE, 1.25 cm, Urgo Medical, Chenôve, France) on Petri dishes (diameter 8.5 cm) and subsequently filled with 25 mL of

BSM. Thirty minutes prior to measurement, the BSM solutions in the petri dishes were changed. Net H^+ fluxes were then measured from the exposed cells using non-invasive H^+-selective scanning microelectrodes. According to (Newman, 2001) and (Dindas *et al.*, 2018), microelectrodes were pulled from unfilamented borosilicate glass capillaries (Ø 1.0 mm, Science Products GmbH, Hofheim, Germany) dried over night at 220 °C, then silanized with N,N-dimethyltrimethylsilylamine (Sigma-Aldrich) for 1 h. The electrodes were subsequently back-filled with a backfilling solution (15 mM NaCl/40 mM KH_2PO_4, pH adjusted to 6.0 using NaOH for H^+) and front-filled with an H^+-selective ionophore cocktail (catalogue number 95291 for H^+, Sigma-Aldrich). Calibration of H^+-selective electrodes was performed at pH 4.0, pH 7.0 and pH 9.0. Electrodes with slope > 50 mV per decade and correlation > 0.999 were used for measurements. After calibration, the electrode was placed at a distance approximately 40 µM from the taproot sample using a SM-17 micromanipulator (Narishige Scientific Instrument Lab) and an upright microscope (Axioskop; Carl Zeiss AG, Oberkochen, Germany). During measurements electrodes were moved between two positions, i.e., close to and away from the sample (40 µm and 140 µm, respectively) at 10 s intervals using a micro-stepping motor driver (US Digital, Vancouver, WA, USA). The difference in the potentials between these two points was recorded with a NI USB 6259 interface (National Instruments), controlled by a custom-made, Labview-based software 'Ion Flux Monitor'. The recorded potential was converted offline into proton flux values using the Labview-based program 'Ion Flux Analyser', Excel 2010 and Origin Pro 2021 software.

Current recordings from *Xenopus laevis* oocytes

The two-electrode voltage-clamp technique was applied to *Xenopus laevis* oocytes injected with complementary RNA coding for BvPMT5a and BvSTP13 essentially as described by (Wittek *et al.*, 2017). A standard bath solution was used for the membrane current recordings: 100 mM KCl, 1 mM $CaCl_2$, 1 mM $MgCl_2$, 1 mM $LaCl_3$, adjusted to 220 mosmol kg^{-1} with D-sorbitol or sucrose. Solutions were adjusted either to pH 5.5 with MES/Tris buffer or to pH 6.5 and pH 7.5 with HEPES/Tris buffer. The following sugar compounds were added to the solutions at the concentrations indicated in the figure legends: L-(+)-arabinose, D-(–)-fructose, L-(-)-fucose, D-(+)-galactose, D-(+)-glucose, glycerol, D-glucuronic acid, D-mannitol, D-(+)-mannose, myo-inositol, D-(+)-raffinose, L-rhamnose, D-sorbitol, sucrose, xylitol. Sugar-induced current responses were determined by subtracting the current responses at the end of sugar application from those before sugar administration. For this, usually 150 ms lasting voltage pulses in the range of 0 to -140 mV were applied in 10-mV decrements

before and during sugar application, starting from a holding voltage of -40 mV. Current responses to sugar application were also determined from continuous recordings at a constant membrane voltage.

To study the temperature dependency of the sugar transporters in oocytes, the bath solution passed through a heat exchanger in contact with peltier elements on which the recording chamber was mounted. The temperature was measured with a small thermistor close to the oocyte. In these experiments, the bath solution for BvPMT5-expressing oocytes contained 75 mM NaCl, 50 mM sucrose, 1 mM $CaCl_2$, 1 mM $MgCl_2$, 1 mM $LaCl_3$ and 10 mM MES/TRIS, pH 4.5. To induce uptake currents, sucrose was replaced by 50 mM D-(+)-glucose. The bath solution for BvSTP13-expressing oocytes contained 96 mM NaCl, 2 mM KCl, 1 mM $CaCl_2$, 1 mM $MgCl_2$, 1 mM $LaCl_3$, 0.5 mM D-sorbitol, and 10 mM Mes/Tris, pH 4.5. To induce uptake currents, D-sorbitol was replaced by 0.5 mM D-(+)-glucose.

Data acquisition and offline analysis were performed using the software programs Patch Master (HEKA Electronik, Lambrecht, Germany), Microsoft Excel, Origin2021 (OriginLab Corporation, Northampton, MA 01060 USA) and IgorPro (Wave Metrics Inc., Lake Oswego, OR, USA).

Molecular cloning of sugar beet transporter

To generate constructs for heterologous expression of fluorophore-labelled or untagged *BvPMT5a* or *BvSTP13*, the corresponding coding sequence was amplified from cDNA of root tissue from cold-treated sugar beets. PCR-amplification of target sequences using the primer pNBI-BvPMT5-f (5'- GGG CTG AGG CTT AAT ATG AGT GAA GGA ACT AAT AAA GCC ATG -3') together with BvPMT5-pNBI16/21-r (5'- ATT CGC TGA GGT TTA GTG ATT GTC ATT TGT AAC AGT AGT ACT A -3'), or pNBI-BvSTP13-f (5'- ATT CGC TGA GGT TTA GTG ATT GTC ATT TGT AAC AGT AGT ACT A -3') together with BvSTP13-pNBI16/21-r (5'- ATT CGC TGA GGT TTA TAG AGC TGC AGC TGC AGC AGA CCC ATT AT -3') yielded PCR-fragments for cloning into pNBI16 (no tag), or pNBI21 (N-terminal fluorophore), respectively. PCR using the primer pairs pNBI-BvPMT5-f and BvPMT5-pNBI22-r (5'- CCA GGC TGA GGT TTA AGT GAT TGT CAT TTG TAA CAG TAG TAC TA -3'), or pNBI-BvHT2-f BvSTP13-pNBI22-r and BvSTP13-pNBI22-r (5'- CCA GGC TGA GGT TTA ATA GAG CTG CAG CAG ACC CAT TAT -3'), removed the stop codon of the transporter CDSs to allow generation of fusions to the N-terminus of the yellow fluorescent Venus (pNBI22), respectively. PCR fragments were directly cloned into the *PacI*-linearized expression vectors (pNBI16, pNBI21, or pNBI22) using the In-Fusion® HD

Cloning Kit (Takara Bio USA, Inc.). Insert sequences were verified by sequencing (Eurofins, Germany).

Phylogenetics of sugar transporters

The phylogenetic relationships *Arabidopsis thaliana* and *Beta vulgaris* PMT and STP transporters were studied by aligning the derived amino acid sequences using the MUSCLE plugin (Edgar, 2004) within Geneious (Biomatters, Inc., San Diego, CA) with default parameters. The alignments were trimmed using trimAl v1.2rev59 (Capella-Gutierrez *et al.*, 2009) using the implemented 'gappyout' algorithm. Phylogenetic reconstruction of the MSA was conducted using IQ-TREE multicore version 2.1.2 (Minh *et al.*, 2020). The best-fit substitution models were LG+G4 and LG+I+G4 for the PMT and STP datasets, respectively, and were selected based on the Bayesian Information Criterion and implemented in the Maximum Likelyhood (ML) tree reconstruction. Branch support was estimated using 1000 replicates and ultrafast bootstrap (Hoang *et al.*, 2018). Consensus trees were finally visualized employing the iTol online tool (https://itol.embl.de/).

3D modeling of BvSTP13 and molecular dynamic analysis of saccharide binding

A 3D homology model of BvSTP13 was obtained based on the crystal structure of *Arabidopsis thaliana* STP10 (PDB entry 6H7D; Paulsen *et al.*, 2019) using the modeling macro hm_build.mcr of the software package YASARA Structure version 20.12.24 (https://www.yasara.org, Krieger and Vriend, 2014; PMID 24996895). Briefly, the amino acid sequence of BvSTP13 covering residues Met1 to Leu537 was aligned to the sequence of STP10 using a PSI-BLAST search against the RCSB databank with a maximum E-value of 0.1 for template consideration. Three potential templates were identified: PDB entries 6H7D (AtSTP10, Paulsen *et al.*, 2019), 4ZW9 (HsGTR3, Deng *et al.*, 2015) and 5C65 (HsGTR3/SLC2A3; Pike A.C.W. *et al.* unpublished), although the latter two exhibited considerably lower scores in YASARA's PSI-Blast search and alignment. For modeling a secondary structure prediction, a target sequence profile was built against related UniRef90 sequences. Fourteen initial homology models were then built using the template AtSTP10 (PDB entry 6H7D), employing five slightly different sequence alignments that differed in the adjustments of loop regions. Of these, two exhibited the best overall Z-scores of -0.432 and -0.465 in the YASARA scoring routine after energy minimization and molecular dynamics refinement. The model used for analysis comprised 505 amino acid residues harboring Gly12 to Ala516, the 11 N-terminal and the 21 C-terminal amino acids were not

modeled because there is no template structure available for these residues. However, from the model it can be assumed that these residues are flexible and adopt a dynamic structure. The final model also contained the glucose moiety present in the original template AtSTP10 (PDB entry 6H7D), which engaged in an identical hydrogen bond pattern with surrounding residues in BvSTP13. This was because all amino acids in close proximity to the glucose moiety are conserved between AtSTP10 and BvSTP13. To obtain further insights into possible saccharide binding and specificity of BvSTP13, the monosaccharide fructose and the disaccharide sucrose were also docked in the saccharide binding site of the model. A short molecular dynamic simulation of the BvSTP13 model placed in a membrane layer with either bound glucose, fructose or sucrose was run using YASARA's macro md_runmembrane.mcr. The hexaoxaicosandiol/PEG moiety that was part of the crystallization solution/condition of the original AtSTP10 crystal and which artificially occupied part of the inner binding cleft partially filled with the glucose molecule was removed before the MD simulation. The membrane region of the BvSTP13 molecule was predicted by YASARA. The BvSTP13 model was then centered in a box with the dimensions 83 x 83 x 113 Å and with the membrane region of the BvSTP13 model placed in the lipid bilayer comprising 159 phosphatidyl-ethanolamine molecules. Water was put above and below the membrane bilayer, sodium and chloride ions were placed at a concentration of 150 mM and to neutralize the protein charges within the box. After energy minimization of the membrane bilayer, the water solvent molecules and ions, an unrestrained molecular dynamic simulation was performed at 298K (25 °C) and constant pressure for 5 (BvSTP13 with glucose bound) and 10 ns (BvSTP13 with sucrose or fructose bound). The MD trajectories were analyzed with YASARA with respect to hydrogen bonding between the saccharide molecules and the sugar transporter.

Results

Sugar uptake in taproots is directly linked to proton influx and membrane depolarization

As soon as sucrose is translocated from the source leaves to the taproot and released from the phloem to the apoplast, sucrose needs to enter the storage parenchyma cells (Lemoine *et al.*, 1988; Godt & Roitsch, 2006). For this, sucrose is most likely translocated across the plasma membrane via H^+-coupled sugar uploaders. To date, insights into *Beta vulgaris* taproot sugar

transport have mostly been gained by classical physiological assays such as uptake of radioactive sugars into tissue slices (*in vivo*) and plasma membrane enriched vesicles (*in vitro*). Based on the ground-breaking findings on *Beta vulgaris* sugar transport gained with taproot slices, we took advantage of the same experimental system. To first visualize cellular sucrose loading in the storage organ, we employed the fluorescent sucrose analog esculin, which is accepted by several sucrose transporters as a substrate for membrane translocation (Gora *et al.*, 2012; Reinders *et al.*, 2012; Abelenda *et al.*, 2019). After prolonged incubation of taproot slices from maturating 14 to 18-week-old sugar beets with esculin for 90 or 180 minutes (Method S1), a strong fluorescent signal was detected around the nucleus (Fig. S1a). This indicates the uptake of esculin from the apoplast into the cytosol of parenchyma cells. The results with this fluorescent ß-glycoside suggest that sucrose transporters are present in the plasma membrane and are capable of shuttling sucrose into the cytosol.

Given that a secondary active rather than a passive transport for apoplastic high-capacity sugar loading of the taproot parenchyma cells is the most likely mechanism, we next investigated the plasma membrane electrical phenomena underlying sucrose and glucose uptake using voltage-recording and ion-selective electrodes. For online recording of sucrose- and glucose-induced changes in H^+ fluxes across the plasma membrane of taproot cells non-invasively, we employed scanning H^+-selective electrodes (cf. Reyer *et al.*, 2020). In taproot slices from 14 to 16-week-old maturating sugar beets, resting parenchyma cells were characterized by H^+ efflux activity, as is expected from the plasma membrane H^+ pump (Fig. 1a). In line with a proton-coupled sugar symporter, administration of both glucose and sucrose (50 mM) resulted in a decreased H^+ efflux for often at least 30 minutes (Fig. 1a, Fig. S2a). During this glucose and sucrose evoked phase, maximum proton fluxes of 25.8 ± 7.2 nmol m^{-2} s^{-1} (n = 11, SEM) and 24.1 ± 7.4 nmol m^{-2} s^{-1} (n = 11, SEM) respectively, were measured. This response indicated that the plasma membrane of the parenchyma cells from slices derived from sugar-accumulating taproots is sucrose and glucose transport competent.

In plant cells, the plasma-membrane proton efflux results from the H^+ pump activity of vanadate sensitive AHA-type H^+-ATPases (cf. Reyer *et al.*, 2020, and references therein). Since sugars are not charged while protons are, one must predict that the phenomenon observed for the H^+ fluxes (Fig. 1a, Fig. S2a) is best explained mechanistically by H^+/sugar co-import. To monitor sugar-induced membrane potential changes, cells of the afore identified sugar-sensitive taproot slices were impaled with voltage recording microelectrodes. The membrane potential was -149.9 ± 3.3 mV (n = 18, SEM) at rest, and transiently depolarized by 48.3 ± 6.1 mV (n = 7, SEM) and 51.6 ± 3.7 mV (n = 6, SEM) upon addition of

50 mM glucose and sucrose, respectively (Fig. 1b, Fig. S2b). Without removal of sugar, the membrane voltage generally slowly relaxed to the pre-stimulus level; a behavior in line with a depolarization and H^+ influx-dependent activation of the H^+-ATPase (Reyer *et al.*, 2020). Taken together, our electrophysiological studies with taproot slices indicate that sugar-accumulating taproot cells are equipped with a proton-pumping moiety that drives H^+-coupled sucrose and glucose transport. These findings raise questions about the molecular nature and sugar specificity of the transporters involved.

Low temperatures stimulate *BvPMT5a* and *BvSTP13* transporter expression in taproots

Possible candidates for mediating the observed sugar/H^+ fluxes across the plasma membrane are likely found among members of the Monosaccharide Transporter (MST) superfamily (Büttner, 2007; Pommerrenig *et al.*, 2018). Of the seven MST subfamilies, only the INT, STP and PMT subfamilies harbor plasma membrane transporters (Scholz-Starke *et al.*, 2003; Klepek *et al.*, 2005; Schneider *et al.*, 2006; Schneider *et al.*, 2007; Klepek *et al.*, 2010; Rottmann *et al.*, 2018). INT subfamily members have been reported as carriers for inositol and other polyols, but not for sucrose (Schneider *et al.*, 2006; Schneider *et al.*, 2007). In contrast, STPs and PMTs exhibit a high specificity for the monosaccharides glucose and fructose (Klepek et al., 2005; Rottman et al., 2018). Astonishingly, the MdSTP13a homolog from apple (*Malus domesticus*) has recently been shown to transport the disaccharide sucrose, in addition to the monosaccharide glucose (Li *et al.*, 2020). In our further sugar beet studies, we therefore concentrated on STPs and PMTs. The *Beta vulgaris* genome encodes 14 putative STP-type transport proteins and five PMTs (Fig. S3). Among these, BvSTP13 and BvPMT5a are of particular interest because their mRNA levels were markedly increased in taproots upon exposure to low temperatures (Fig. S4, Method S2). These data suggest a possible role for these two transporters in the taproot tissue of sugar beet during the cold stress response.

BvPMT5a is a proton-coupled glucose and polyol transporter

To gain insights into the possible role of BtPMT5a in taproot sugar uptake and in relation to the electrophysiological *in vivo* recordings from the taproot slices (Fig. 1, Fig. S2), the transport features of BvPMT5a were analyzed in *Xenopus laevis* oocytes via voltage-clamp recordings (Carpaneto *et al.*, 2005; Nieberl *et al.*, 2017). When BvPMT5a-expressing oocytes were exposed to the disaccharide sucrose (10 mM) at pH 5.5 and a membrane voltage of -40 mV, no additional current to the current background noise was elicited. However, application of glucose or fructose caused similar pronounced inward currents (Fig. 2a, b). In addition to

the monosaccharides released by sucrose breakdown via invertase activity, BvPMT5a-expressing oocytes were challenged with the glucose derivative glucuronic acid, hexose deoxy sugars fucose and rhamnose, pentose arabinose, and various polyols (sorbitol, mannitol, myo-inositol, glycerol, xylitol). Among these, mannitol, glucuronic acid and glycerol only produced very weak inward currents. Sorbitol, arabinose, fucose, rhamnose and myo-inositol induced similar currents to glucose and fructose, while xylitol caused the largest current response (Fig. 2b). This behavior of BvPMT5a points to a transporter of broad substrate specificity. Due to the favorable signal-to-background-noise ratio with xylitol as a BvPMT5a substrate, this polyol was selected as a representative substrate to study the involvement of protons as a potential co-substrate in the translocation process. As expected from a H^+-driven monosaccharide/polyol transporter, in the presence of 10 mM xylitol polyol-induced inward currents became smaller when at a membrane voltage of -40 mV, the external pH was increased, and the proton motive force (PMF) was decreased in steps from 5.5 to 6.5 and 7.5 (Fig. S5a). At a membrane voltage of 0 mV and pH of 7.5, a value where the extracellular and cytosolic proton concentrations match, the PMF is zero (Fig. S5b). Nevertheless, polyol application still elicited inward currents that reached about 25% of those driven by a 100-fold H^+ gradient at pH 5.5 (Fig. S5b). In the absence of a PMF, H^+ uptake into the cell was driven solely by the polyol concentration gradient directed into the cytosol. When the membrane voltage became increasingly hyperpolarized, the PMF increased, resulting in larger inward currents under any pH situation. However, at voltages more negative than -80 mV, the xylitol-induced currents measured at pH 6.5 and 5.5 became very similar, suggesting that the maximal transport capacity reached a similar level under both pH conditions and is no longer promoted by the voltage part of the PMF. When instead of the external pH, the xylitol concentration was varied by adding either 1, 3, 5, 10, 20, 30, 50 or 100 mM xylitol, the inward current increased stepwise from a concentration of 1 to 20 mM, saturating above 30 mM (Fig. 3a,b). This saturation behavior could be fitted with a Michaelis-Menten function from which a K_m value of 2.5 mM was derived (Fig. 3b,c). When the electrical driving force was increased from -40 to -140 mV, reflecting the resting membrane voltage of the taproot parenchyma cells (Fig. 1b, Fig. S2b), the affinity to this polyol substrate increased almost two-fold as the K_m dropped from 2.5 to 1.5 mM (Fig. 3c). In analogous experiments involving the glucose-dose dependency of BvPMT5a (Fig. 3d-f), the derived K_m values for glucose also decreased (Fig. 3e,f), indicating that the PMF is energizing the BvPMT5a H^+/glucose cotransport. This identifies BvPMT5a as a potential candidate for glucose uploading in beet roots.

BvSTP13 operates as a high-affinity, proton-coupled glucose and sucrose transporter

Like BvPMT5a, BvSTP13 was heterologously expressed and its transport features characterized in *Xenopus laevis* oocytes. At an external pH of 5.5 and a membrane potential of -40 mV, BvSTP13-expressing oocytes were exposed to various monosaccharides as well as to di- and trisaccharides (Fig. 4a). Upon application of 10 mM hexose quantities, BvSTP13-mediated inward currents of similar large amplitudes were recorded with glucose, fructose, galactose and mannose. In contrast, the polyols sorbitol, myo-inositol and xylitol, the hexoses rhamnose and fucose, the pentose arabinose and the hexose derivative glucuronic acid all caused no or only small currents. The aldopentose xylose, however, triggered current responses that reached approximately 70% of those obtained with glucose. When exposed to the glucose-fructose disaccharide sucrose, similar pronounced inward currents to those with xylose were obtained. Unexpectedly, even the trisaccharide raffinose evoked current responses of amplitudes that were still about 40% of those reached with glucose. BvSTP13 also accepted the sucrose surrogate esculin as a substrate (Fig. S6a). These current responses demonstrate that BvSTP13 is not a typical hexose transporter; it is capable of transporting not only certain monosaccharides but also sucrose and raffinose.

To determine the glucose-dose dependency of the BvSTP13 transporter, the glucose concentration was increased stepwise from 0.05 mM to 1.0 mM (Fig. 4b). In these experiments, inward currents were evoked with as little as 0.05 mM glucose. Currents tended to saturate when the substrate concentration was raised above 0.1 mM (Fig. 4b,c). The K_m value at a membrane potential of -40 mV for glucose was 0.075 mM (Fig. 4c,d), indicating that BvSTP13 represents a high-affinity sugar transporter. Like glucose, the application of sucrose elicited H^+ inward currents at a concentration as low as 0.05 mM (Fig. 6a,b), suggesting that BvSTP13 also has a high affinity to sucrose. At the glucose and sucrose concentrations tested, membrane hyperpolarization and an acidic external pH enhanced the inward currents (Fig. 4e, Fig. S6b,c, Fig. S7). Together, the voltage and pH dependency of the BvSTP13-mediated currents demonstrate that as with BvPMT5a, the BvSTP13-mediated sugar translocation is proton-coupled, so thermodynamically driven by the proton motive force and the sugar gradient (cf. Carpaneto *et al.*, 2005; Reinders *et al.*, 2005; Wittek *et al.*, 2017). However, in contrast to BvPMT5a (Fig. 3f), the K_m values of BvSTP13 for glucose surprisingly increased to about 0.16 mM upon hyperpolarization to -140 mV. This indicates that BvPMT5a gains a higher sugar affinity when the membrane potential is depolarized.

BvPMT5a and BvSTP13 were noticed because they become transcriptionally up-regulated upon exposure to low temperatures (Fig. S4). Thus, in addition to parameters such as the PMF and voltage dependence, we asked how carrier function and thermodynamics respond to temperature changes. In the Xenopus oocyte system, the temperature was lowered from 35 to 5 °C in 10 °C steps, and the glucose-induced current responses were monitored (Fig. 5). Current amplitudes with both transporters decreased with each cooling step. However, BvPMT5a-mediated currents could only be resolved when the temperature was raised above 5 °C. Above this temperature threshold, warming up the oocyte by 10 °C steps increased the transporter activity with a Q_{10} of about 4. In contrast, significant BvSTP13-related currents were recorded already at 5 °C and were characterized by a Q_{10} of about 2.

Modeling the BvSTP13 structure with bound mono- and disaccharide

To obtain the first insights into the molecular nature of the broad sugar specificity of BvSTP13, we modeled BvSTP13, based on the known structure of the monosaccharide transporter AtSTP10 from *Arabidopsis thaliana* (Rottmann *et al.*, 2016; Paulsen *et al.*, 2019; Bavnhøj *et al.*, 2021). In accordance with their shared overall 6TM-loop-6TM topology (TM, transmembrane domain), the BvSTP13 amino acid sequence could be perfectly mapped onto the AtSTP10 structure (Fig. S8). The 3D model obtained for BvSTP13 revealed all the structural hallmarks of the STP protein family. This includes the existence of a characteristic 'lid-domain' covering the extracellular entry pathway to the sugar binding site, and a cavity that is formed between the N-terminal and C-terminal halves of the sugar transporter (Fig. S8a). The structural alignment further revealed that core amino acid residues, identified as constituting the binding sites for coordinating the glucose substrate (Paulsen *et al.*, 2019), were perfectly conserved between both transporters, with the exception of Leu43 in AtSTP10, which is replaced conservatively by valine (Val44) in BvSTP13 (Fig. S8b). The presence of a hydrophilic polyethylene glycol (PEG) moiety above the bound glucose molecule in the AtSTP10 structure and resulting (artificially) from the crystallization conditions indicates that the saccharide binding cleft in the determined outward open conformation is wide enough to accommodate carbohydrates larger than monosaccharides (Fig. 6). In our model of BvSTP13 bound with sucrose, space for the second carbohydrate moiety of the disaccharide is provided by changes in the sidechain conformation of Asn304 and Met307. This suggests that the spatial requirements of sucrose accommodation could seemingly be fulfilled in BvSTP13 as well as in AtSTP10. A molecular dynamics (MD) simulation of our BvSTP13 model placed in an explicit solvent/membrane bilayer and having either a glucose or sucrose molecule

bound did not provide hints as to why BvSTP13 should exhibit stringent specificity for binding either glucose or sucrose (Fig. 6).

The proton donor/acceptor residue pair needed for proton translocation, Asp42 and Arg142 in AtSTP10, is preserved in BvSTP13 as well as in the polyol transporter BvPMT5a. However, amino acid residues involved in substrate coordination partially differ between polyol and sugar transporters. Markedly, BvPMT5a lacks a 'lid domain' (Fig. S9). Specific for members of the STP family, this 'lid domain' connects the N- and C-terminal moieties of the transporter via a disulfide bridge. Recent work by Bavnhøj et. al (2021) shows that following sugar binding and protonation of the Asp42 the 'lid domain' undergoes dramatic structural rearrangements and isolates the protonation site from the apoplast to define an outward occluded state. During transition to an inward open state the 'lid domain' moves again and – via the conserved disulfide bond - locks the central helices of the N- and C-terminal transmembrane domains together, isolating both the protonation and the sugar biding site binding site from the extracellular space. Our modeling approach revealed that the 'lid domain' differs between AtSTP10 and BvSTP13, in particular, the non-structured loop C-terminal to the two short helices in the apoplastic loop between TM1 and TM2 (Fig. S8a).

Discussion

BvPMT5a and BvSTP13 together function as low and high-affinity proton-driven glucose importers

To discover the solute moiety transported by the phloem *in vivo*, aphid stylectomy was used to identify sucrose as the major sugar (Fisher *et al.*, 1992). Furthermore, aphid stylectomy in combination with electrophysiology revealed that sucrose-uptake into the phloem depolarizes the membrane potential of the sieve elements (Carpaneto *et al.*, 2005). Sucrose in the plant is disseminated from source to sink via the phloem network. In sink organs such as a taproot in the case of sugar beet, sucrose exits the phloem apoplastically (Lemoine *et al.*, 1988; Godt & Roitsch, 2006). However, depending on the activity of extracellular invertase at the exit site (Lemoine *et al.*, 1988; Jammer *et al.*, 2020), parenchyma sugar transporters will be faced with glucose and fructose in addition to sucrose. Our electrophysiological studies with taproot parenchyma cells clearly demonstrate that the plasma membrane responds to glucose and sucrose, as expected from transporter-mediated proton-driven sugar import (Fig. 1, Fig. S2). Two cold-associated transporters BvPMT5a and BvSTP13 were characterized in the oocyte

system as H^+/solute symporters (Figs 2-5, Figs S5-7). BvPMT5a mediates the proton-coupled import of glucose with a millimolar affinity (Fig. 3). BvSTP13 shuttles both glucose and sucrose with submillimolar affinities (Fig. 4, Fig. S6a,b), probably similar to AtSTP1 with a 1:1 stoichiometry in cotransport with a proton (Boorer *et al.*, 1994). Thus together, BvPMT5a and BvSTP13 provide for high and low-affinity glucose uptake (Figs 3f, 4d). Whether the opposite weak voltage dependency of the BvSTP13 glucose affinity is correlated with a spatial rearrangement of substrate binding sites during the transport cycle conferred by the 'Lid domain' – present in BvSTP13 but absent in BvPMT5a (Fig. S9) – needs to be explored in further studies. That (i) taproot parenchyma cells import esculin, (ii) according to MD simulations, BvSTP13 is capable of binding glucose, sucrose and esculin, and (iii) in electrophysiological experiments, BvSTP13, like the apple MdSTP13a in radioactive tracer experiments (Li *et al.*, 2020), was demonstrated to transport not only glucose and fructose but also sucrose and esculin, suggests that this symporter is involved in the loading of monosaccharides and possibly sucrose as well, into storage parenchyma cells.

How to fit glucose and sucrose in the same transporter?

The crystal structure of a member of the monosaccharide transporter superfamily, AtSTP10 with glucose bound, provided molecular insights into the hexose uptake mechanism (Paulsen *et al.*, 2019). In contrast to the PMTs, a lid domain, which is conserved in all STPs, shields both the sugar binding site and the proton binding site from the extracellular lumen. We used homology models for BvSTP13 and MdSTP13a (Li *et al.*, 2020) and in silico docking of various saccharides to unravel how possible differences in saccharide binding in different members of the STP sugar transporter family might explain their observed substrate specificity (Fig. 6, Fig. S8). In line with their similar saccharide specificity, all amino acid residues in the binding cleft of the STP13 sugar transporter from sugar beet and apple (Li *et al.*, 2020) were conserved within an 8 Å sphere of the glucose moiety position as found in AtSTP10. Likewise, in this region only three amino acids differ between AtSTP10 and BvSTP13, all other residues are identical (see also Fig. S8b). Based on the presence of three water molecules and a hydrophilic polyethylene glycol molecule in the binding cleft just above the glucose moiety, our MD simulations suggest that the binding site exhibits plasticity. This binding cleft plasticity could allow to accommodate di- and trisaccharides in BvSTP13 (and possibly AtSTP10). The three amino acids, that differ between AtSTP10 and BvSTP13 are located below a conserved tryptophan (Trp410 and Trp412 in AtSTP10 and BvSTP13, respectively). This residue resides beneath the saccharide binding cleft occupied by glucose

and can be considered a kind of dead-end of the sugar accommodating cavity. In the structurally determined outward-open conformation (Paulsen *et al.*, 2019), the bulky indole ring of Trp410 in AtSTP10 prevents further downward movement of the glucose towards the transporters' cytoplasmic face. Because information on other required structural transporter conformations is currently not available and that there is an apparent lack of difference in the sugar binding, we cannot predict how these different residues affect saccharide binding or transport specificity. Thus, the currently available structure (of only the outward open conformation) (Paulsen *et al.*, 2019) can only provide insights into the binding situation when the saccharide moiety enters the cleft and is coordinated at the glucose binding site. Neither data for the transfer of the saccharide past the lid domain to the binding site nor for structural changes in the transport protein accompanying their further translocation from the binding cleft to the cytoplasmic site are available. The available structurally resolved conformations of the Arabidopsis STP10 transporter together with molecular modelling and MD simulations provides for testable predictions towards key residues determining sugar coordination and substrate specificity during the transport cycle. Future work based on mutagenesis and structure-function studies needs to elucidate whether the carbohydrate specificity of STP transporters is determined by the binding site itself or is attributable to conformational changes during their predicted outward open to inward open transport cycle.

BvPMT5a and BvSTP13 with a possible role in cold response

As with the plasma membrane sugar transporters BvPMT5a and BvSTP13, the expression of the vacuolar Arabidopsis TONOPLAST SUGAR TRANSPORTERS TST1 and TST2 are induced by low temperatures (Wormit *et al.*, 2006). During cold acclimation, *tst1/2* knockout lines exhibited elevated sucrose levels, but reduced glucose and fructose levels in the leaves compared with wild-type plants. This affected cold tolerance (Wormit *et al.*, 2006; Klemens *et al.*, 2014); the cellular sugar content contributes to cold hardening. Together with their transcriptional induction by cold, these observations suggest that for cold tolerance of the sugar beet taproot, BvSTP13- and BvPMT5a-mediated plasma membrane hexose transport may be important. In addition to sugars, polyols are also cold protective in nature, and these are also substrates of BvPMT5a. Therefore, BvPMT5a and BvSTP13 together could provide root parenchyma cells with cold protective compounds. Further studies will have to answer this question. Functional expression of BvPMT5a and BvSTP13 in e.g. *Arabidopsis* wild type and loss-of-sugar-transport-function mutants of the PMT5 and STP13 sub-clades (see Fig. S2) will allow to study their impact on cold stress induced changes in plant/cell sugar levels and

profiles as well as their overall contribution to freezing tolerance (Jung et al. (2015), Wang et al. (2020) Nieberl et al. (2017) and Ho et al. (2019)).

In summary, our manuscript provides a gain in knowledge regarding the molecular identification of prime sugar transporter candidates of tap root cells. Our functional studies underline that these two transporters are strong candidates for the two different classes of monosaccharide transporters in *Beta vulgaris*. Additionally, we identified that BvSTP13 is also capable of transporting sucrose as a disaccharide as well as transporting monosaccharides. This astonishing finding could be underlined *in silico* by structure modelling bound with substrate. This model provides us a testable hypothesis for the molecular mechanism of the transport of glucose and sucrose by a member from a monosaccharide transporter family. Given that the temperature activity profiles of the two sugar transporters overlap, with BvSTP13 being more cold-resistant than BvPMT5a, it is tempting to speculate that during cold acclimation, these H^+ symporters work hand in hand.

Acknowledgements

This work was funded by a research grant to R.H. and H.E.N. by the Federal Ministry of Education and Research (project 'Betahiemis', FKZ 031B0185) and a King Saud University to R.H., K.A.S.A., A.H.A. and S.A.A. (Project ICSTD-2020/2). W.K. and F.L. are employees of KWS SAAT SE (Einbeck, Germany) and K.H. is an employee of Südzucker AG (Obrigheim/Pfalz, Germany). We thank Fábio Luiz Rogé Ferreira for his help in collecting raw electrophysiological data in Xenopus oocytes and Christina Müdsam for cloning of the sugar beet transporters.

Author Contributions

R.H., I.M., H.E.N., K.H., W.K., F.L. designed the research; A.R., J.J., N.B., N.S., S.S. performed research; A.R., D.J., J.J., N.B., N.S., T.D.M., D.B., S.S. analyzed data and R.H., I.M, D.B., T.D.M., K.A.S.A.-R., A.H.A., S.A.A., A.R., T.A.C., B.P., H.E.N. wrote the paper.

Data Availability

The data that support the electrophysiological/phylogenetic/structural findings and the RNA analysis of this study are available upon request from the corresponding author and Benjamin Pommerrening, respectively. RNA-seq data are found in the GenBank Sequence Read Archive (BioProject PRJNA602804).

Funding

This work was funded by a research grant to R.H. and H.E.N. by the Federal Ministry of Education and Research (project 'Betahiemis', FKZ 031B0185) and a King Saud University to R.H., K.A.S.A., A.H.A. and S.A.A. (Project ICSTD-2020/2). W.K. and F.L. are employees of KWS SAAT SE (Einbeck, Germany) and K.H. is an employee of Südzucker AG (Obrigheim/Pfalz, Germany).

Conflict of interest statement. None declared.

REFERENCES

Abelenda JA, Bergonzi S, Oortwijn M, Sonnewald S, Du M, Visser RGF, Sonnewald U, Bachem CWB. 2019. Source-Sink Regulation Is Mediated by Interaction of an FT Homolog with a SWEET Protein in Potato. *Curr Biol* **29**(7): 1178-1186 e1176.

Bavnhøj L, Paulsen PA, Flores-Canales JC, Schiøtt B, Pedersen BP. 2021. Molecular mechanism of sugar transport in plants unveiled by structures of glucose/H^+ symporter STP10. *Nature Plants*.

Boorer KJ, Loo DD, Wright EM. 1994. Steady-state and presteady-state kinetics of the H^+/hexose cotransporter (STP1) from Arabidopsis thaliana expressed in Xenopus oocytes. *J Biol Chem* **269**(32): 20417-20424.

Buckhout TJ. 1989. Surcose transport in isolated plasma-membrane vesicles from sugar beet (Beta vulgaris L.) Evidence for an electrogenic sucrose-proton symport. *Planta* **178**(3): 393-399.

Bush DR. 1989. Proton-Coupled Sucrose Transport in Plasmalemma Vesicles Isolated from Sugar Beet (*Beta vulgaris* L. cv Great Western) Leaves. *Plant Physiol* **89**(4): 1318-1323.

Bush DR. 1990. Electrogenicity, pH-Dependence, and Stoichiometry of the Proton-Sucrose Symport. *Plant Physiol* **93**(4): 1590-1596.

Büttner M. 2007. The monosaccharide transporter (-like) gene family in Arabidopsis. *FEBS Letters* **581**(12): 2318-2324.

Capella-Gutierrez S, Silla-Martinez JM, Gabaldon T. 2009. trimAl: a tool for automated alignment trimming in large-scale phylogenetic analyses. *Bioinformatics* **25**(15): 1972-1973.

Carpaneto A, Geiger D, Bamberg E, Sauer N, Fromm J, Hedrich R. 2005. Phloem-localized, proton-coupled sucrose carrier ZmSUT1 mediates sucrose efflux under the control of the sucrose gradient and the proton motive force. *J Biol Chem* **280**(22): 21437-21443.

Deng D, Sun P, Yan C, Ke M, Jiang X, Xiong L, Ren W, Hirata K, Yamamoto M, Fan S, et al. 2015. Molecular basis of ligand recognition and transport by glucose transporters. *Nature* **526**(7573): 391-396.

Dindas J, Scherzer S, Roelfsema MRG, von Meyer K, Muller HM, Al-Rasheid KAS, Palme K, Dietrich P, Becker D, Bennett MJ, et al. 2018. AUX1-mediated root hair auxin influx governs $SCF^{TIR1/AFB}$-type Ca^{2+} signaling. *Nat Commun* **9**(1): 1174.

Dohm JC, Minoche AE, Holtgrawe D, Capella-Gutierrez S, Zakrzewski F, Tafer H, Rupp O, Sorensen TR, Stracke R, Reinhardt R, et al. 2014. The genome of the recently domesticated crop plant sugar beet (*Beta vulgaris*). *Nature* **505**(7484): 546-549.

Edgar RC. 2004. MUSCLE: multiple sequence alignment with high accuracy and high throughput. *Nucleic Acids Res* **32**(5): 1792-1797.

Fieuw S, Willenbrink J. 1990. Sugar transport and sugar-metabolizing enzymes in sugar beet storage roots (*Beta vulgaris* ssp. altissima). *Journal of Plant Physiology* **137**(2): 216-223.

Fisher DB, Wu Y, Ku MS. 1992. Turnover of soluble proteins in the wheat sieve tube. *Plant Physiol* **100**(3): 1433-1441.

Godt D, Roitsch T. 2006. The developmental and organ specific expression of sucrose cleaving enzymes in sugar beet suggests a transition between apoplasmic and symplasmic phloem unloading in the tap roots. *Plant Physiol Biochem* **44**(11-12): 656-665.

Gora PJ, Reinders A, Ward JM. 2012. A novel fluorescent assay for sucrose transporters. *Plant methods* **8**: 13-13.

Gurel E, Gurel S, Lemaux PG. 2008. Biotechnology Applications for Sugar Beet. *Critical Reviews in Plant Sciences* **27**(2): 108-140.

Gusta LV, Wisniewski M, Nesbitt NT, Gusta ML. 2004. The effect of water, sugars, and proteins on the pattern of ice nucleation and propagation in acclimated and nonacclimated canola leaves. *Plant Physiol* **135**(3): 1642-1653.

Ho L-H, Klemens PAW, Neuhaus HE, Ko H-Y, Hsieh S-Y, Guo W-J. 2019. SlSWEET1a is involved in glucose import to young leaves in tomato plants. *Journal of Experimental Botany* **70**(12): 3241-3254.

Hoang DT, Chernomor O, von Haeseler A, Minh BQ, Vinh LS. 2018. UFBoot2: Improving the Ultrafast Bootstrap Approximation. *Mol Biol Evol* **35**(2): 518-522.

Jammer A, Albacete A, Schulz B, Koch W, Weltmeier F, van der Graaff E, Pfeifhofer HW, Roitsch TG. 2020. Early-stage sugar beet taproot development is characterized by three distinct physiological phases. *Plant Direct* **4**(7): e00221.

Jung B, Ludewig F, Schulz A, Meißner G, Wöstefeld N, Flügge U-I, Pommerrenig B, Wirsching P, Sauer N, Koch W, et al. 2015. Identification of the transporter responsible for sucrose accumulation in sugar beet taproots. *Nature Plants* **1**(1): 14001.

Klemens PA, Patzke K, Trentmann O, Poschet G, Buttner M, Schulz A, Marten I, Hedrich R, Neuhaus HE. 2014. Overexpression of a proton-coupled vacuolar glucose exporter impairs freezing tolerance and seed germination. *New Phytol* **202**(1): 188-197.

Klepek YS, Geiger D, Stadler R, Klebl F, Landouar-Arsivaud L, Lemoine R, Hedrich R, Sauer N. 2005. Arabidopsis POLYOL TRANSPORTER5, a new member of the monosaccharide transporter-like superfamily, mediates H^+-Symport of numerous substrates, including myo-inositol, glycerol, and ribose. *Plant Cell* **17**(1): 204-218.

Klepek YS, Volke M, Konrad KR, Wippel K, Hoth S, Hedrich R, Sauer N. 2010. Arabidopsis thaliana POLYOL/MONOSACCHARIDE TRANSPORTERS 1 and 2:

687 fructose and xylitol/H^+ symporters in pollen and young xylem cells. *J Exp Bot* **61**(2):
688 537-550.
689 **Krasensky J, Jonak C. 2012.** Drought, salt, and temperature stress-induced metabolic
690 rearrangements and regulatory networks. *J Exp Bot* **63**(4): 1593-1608.
691 **Krieger E, Vriend G. 2014.** YASARA View - molecular graphics for all devices - from
692 smartphones to workstations. *Bioinformatics* **30**(20): 2981-2982.
693 **Lemoine R, Daie J, Wyse R. 1988.** Evidence for the Presence of a Sucrose Carrier in
694 Immature Sugar Beet Tap Roots *Plant Physiology* **86**(2): 575-580.
695 **Li C, Meng D, Piñeros MA, Mao Y, Dandekar AM, Cheng L. 2020.** A Sugar Transporter
696 Takes Up both Hexose and Sucrose for Sorbitol-Modulated In Vitro Pollen Tube
697 Growth in Apple. *The Plant Cell* **32**(2): 449.
698 **Michonneau P, Roblin G, Bonmort J, Fleurat-Lessard P. 2004.** Valine uptake in the tap
699 root of sugar beet: a comparative analysis with sucrose uptake. *J Plant Physiol*
700 **161**(12): 1299-1314.
701 **Minh BQ, Schmidt HA, Chernomor O, Schrempf D, Woodhams MD, von Haeseler A,**
702 **Lanfear R. 2020.** IQ-TREE 2: New Models and Efficient Methods for Phylogenetic
703 Inference in the Genomic Era. *Mol Biol Evol* **37**(5): 1530-1534.
704 **Newman IA. 2001.** Ion transport in roots: measurement of fluxes using ion-selective
705 microelectrodes to characterize transporter function. *Plant Cell Environ* **24**(1): 1-14.
706 **Nieberl P, Ehrl C, Pommerrenig B, Graus D, Marten I, Jung B, Ludewig F, Koch W,**
707 **Harms K, Flügge U-I, et al. 2017.** Functional characterisation and cell specificity of
708 BvSUT1, the transporter that loads sucrose into the phloem of sugar beet (*Beta*
709 *vulgaris* L.) source leaves. *Plant Biology* **19**(3): 315-326.
710 **Paulsen PA, Custódio TF, Pedersen BP. 2019.** Crystal structure of the plant symporter
711 STP10 illuminates sugar uptake mechanism in monosaccharide transporter
712 superfamily. *Nature Communications* **10**(1): 407.
713 **Pommerrenig B, Ludewig F, Cvetkovic J, Trentmann O, Klemens PAW, Neuhaus HE.**
714 **2018.** In Concert: Orchestrated Changes in Carbohydrate Homeostasis Are Critical for
715 Plant Abiotic Stress Tolerance. *Plant and Cell Physiology* **59**(7): 1290-1299.
716 **Poschet G, Hannich B, Raab S, Jungkunz I, Klemens PA, Krueger S, Wic S, Neuhaus**
717 **HE, Buttner M. 2011.** A novel Arabidopsis vacuolar glucose exporter is involved in
718 cellular sugar homeostasis and affects the composition of seed storage compounds.
719 *Plant Physiol* **157**(4): 1664-1676.
720 **Reinders A, Panshyshyn JA, Ward JM. 2005.** Analysis of transport activity of Arabidopsis
721 sugar alcohol permease homolog AtPLT5. *J Biol Chem* **280**(2): 1594-1602.
722 **Reinders A, Sivitz AB, Ward JM. 2012.** Evolution of plant sucrose uptake transporters.
723 *Front Plant Sci* **3**: 22.
724 **Reyer A, Häßler M, Scherzer S, Huang S, Pedersen JT, Al-Rasheid KAS, Bamberg E,**
725 **Palmgren M, Dreyer I, Nagel G, et al. 2020.** Channelrhodopsin-mediated
726 optogenetics highlights a central role of depolarization-dependent plant proton pumps.
727 *Proceedings of the National Academy of Sciences* **117**(34): 20920-20925.
728 **Riesmeier JW, Willmitzer L, Frommer WB. 1992.** Isolation and characterization of a
729 sucrose carrier cDNA from spinach by functional expression in yeast. *EMBO J*
730 **11**(13): 4705-4713.
731 **Rodrigues CM, Müdsam C, Keller I, Zierer W, Czarnecki O, Corral JM, Reinhardt F,**
732 **Nieberl P, Fiedler-Wiechers K, Sommer F, et al. 2020.** Vernalization Alters Sink
733 and Source Identities and Reverses Phloem Translocation from Taproots to Shoots in
734 Sugar Beet. *The Plant Cell* **32**(10): 3206-3223.
735 **Rodrigues CM, Mudsam C, Keller I, Zierer W, Czarnecki O, Corral JM, Reinhardt F,**
736 **Nieberl P, Fiedler-Wiechers K, Sommer F, et al. 2020.** Vernalization Alters Sink

737 and Source Identities and Reverses Phloem Translocation from Taproots to Shoots in
738 Sugar Beet. *Plant Cell* **32**(10): 3206-3223.
739 **Rottmann T, Fritz C, Sauer N, Stadler R. 2018.** Glucose Uptake via STP Transporters
740 Inhibits in Vitro Pollen Tube Growth in a HEXOKINASE1-Dependent Manner in
741 Arabidopsis thaliana. *Plant Cell* **30**(9): 2057-2081.
742 **Rottmann T, Zierer W, Subert C, Sauer N, Stadler R. 2016.** STP10 encodes a high-
743 affinity monosaccharide transporter and is induced under low-glucose conditions in
744 pollen tubes of Arabidopsis. *J Exp Bot* **67**(8): 2387-2399.
745 **Saftner RA, Daie J, Wyse RE. 1983.** Sucrose Uptake and Compartmentation in Sugar Beet
746 Taproot Tissue *Plant Physiology* **72**(1): 1-6.
747 **Saftner RA, Wyse RE. 1980.** Alkali Cation/Sucrose Co-transport in the Root Sink of Sugar
748 Beet. *Plant Physiology* **66**(5): 884-889.
749 **Sakr S, Lemoine R, Gaillard C, Delrot S. 1993.** Effect of cutting on solute uptake by
750 plasma membrane vesicles from sugar beet (*Beta vulgaris* L.) leaves. *Plant Physiol*
751 **103**(1): 49-58.
752 **Sauer N, Friedlander K, Graml-Wicke U. 1990.** Primary structure, genomic organization
753 and heterologous expression of a glucose transporter from *Arabidopsis thaliana*.
754 *EMBO J* **9**(10): 3045-3050.
755 **Sauer N, Tanner W. 1989.** The hexose carrier from Chlorella. cDNA cloning of a eucaryotic
756 H^+-cotransporter. *FEBS Lett* **259**(1): 43-46.
757 **Schneider S, Hulpke S, Schulz A, Yaron I, Holl J, Imlau A, Schmitt B, Batz S, Wolf S,**
758 **Hedrich R, et al. 2012.** Vacuoles release sucrose via tonoplast-localised SUC4-type
759 transporters. *Plant biol (Stuttg)* **14**(2): 325-336.
760 **Schneider S, Schneidereit A, Konrad KR, Hajirezaei MR, Gramann M, Hedrich R,**
761 **Sauer N. 2006.** Arabidopsis INOSITOL TRANSPORTER4 mediates high-affinity H^+
762 symport of myoinositol across the plasma membrane. *Plant Physiol* **141**(2): 565-577.
763 **Schneider S, Schneidereit A, Udvardi P, Hammes U, Gramann M, Dietrich P, Sauer N.**
764 **2007.** Arabidopsis INOSITOL TRANSPORTER2 mediates H^+ symport of different
765 inositol epimers and derivatives across the plasma membrane. *Plant Physiol* **145**(4):
766 1395-1407.
767 **Scholz-Starke J, Buttner M, Sauer N. 2003.** AtSTP6, a new pollen-specific H^+-
768 monosaccharide symporter from Arabidopsis. *Plant Physiol* **131**(1): 70-77.
769 **Schulz A, Beyhl D, Marten I, Wormit A, Neuhaus E, Poschet G, Buttner M, Schneider S,**
770 **Sauer N, Hedrich R. 2011.** Proton-driven sucrose symport and antiport are provided
771 by the vacuolar transporters SUC4 and TMT1/2. *Plant J* **68**(1): 129-136.
772 **Tarkowski LP, Van den Ende W. 2015.** Cold tolerance triggered by soluble sugars: a
773 multifaceted countermeasure. *Front Plant Sci* **6**: 203.
774 **Wang Z, Wei X, Yang J, Li H, Ma B, Zhang K, Zhang Y, Cheng L, Ma F, Li M. 2020.**
775 Heterologous expression of the apple hexose transporter MdHT2.2 altered sugar
776 concentration with increasing cell wall invertase activity in tomato fruit. *Plant*
777 *biotechnology journal* **18**(2): 540-552.
778 **Wanner LA, Junttila O. 1999.** Cold-induced freezing tolerance in Arabidopsis. *Plant*
779 *Physiol* **120**(2): 391-400.
780 **Wittek A, Dreyer I, Al-Rasheid KAS, Sauer N, Hedrich R, Geiger D. 2017.** The fungal
781 UmSrt1 and maize ZmSUT1 sucrose transporters battle for plant sugar resources. *J*
782 *Integr Plant Biol* **59**(6): 422-435.
783 **Wormit A, Trentmann O, Feifer I, Lohr C, Tjaden J, Meyer S, Schmidt U, Martinoia E,**
784 **Neuhaus HE. 2006.** Molecular identification and physiological characterization of a
785 novel monosaccharide transporter from Arabidopsis involved in vacuolar sugar
786 transport. *Plant Cell* **18**(12): 3476-3490.

787 **Wyse R. 1979.** Sucrose Uptake by Sugar Beet Tap Root Tissue. *Plant Physiology* **64**(5): 837-
788 841.

789

Figures

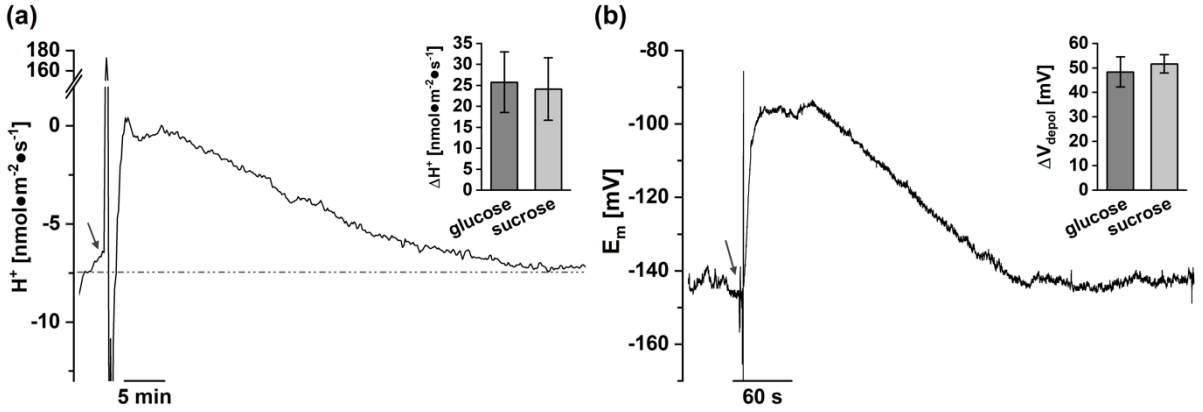

Fig. 1 Glucose- and sucrose-induced changes in H^+ fluxes and membrane depolarization of *Beta vulgaris* taproot cells. (a) H^+ flux trace recorded from taproot slices in response to 50 mM glucose treatment. Time of glucose application is denoted by the arrow. Negative and positive fluxes represent H^+ release from the cells and H^+ uptake into the cells, respectively. The H^+ flux level determined at rest shortly before sugar administration is indicated by a dotted line. The bar graph shows the maximal glucose- and sucrose-induced changes in the H^+ fluxes relative to the H^+ flux level at rest. Data represent means ± SEM with n = 11 each for glucose and sucrose. (b) Free running membrane voltage trace recorded from a taproot slice in response to 50 mM glucose. Time of glucose application is indicated by the arrow. The bar graph shows the maximal glucose- and sucrose-induced depolarization of the slices. Data represent means ± SEM of seven or six different taproots for glucose and sucrose, respectively. In (a), (b) taproots from GT2 were used.

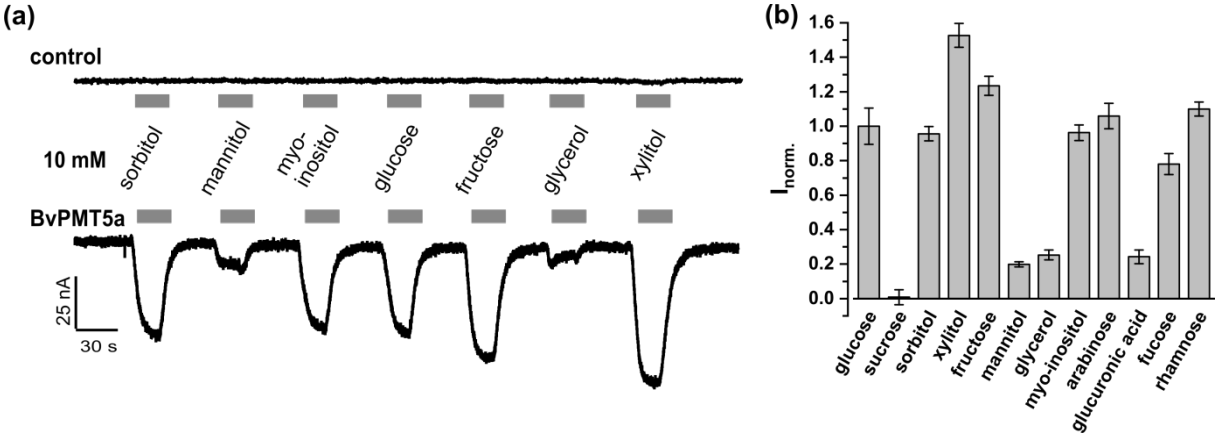

Fig. 2 Substrate specificity of BvPMT5a. (a) Representative macroscopic current recordings of *Xenopus laevis* oocytes injected either with water (control) or BvPMT5a complementary RNA. Currents were recorded at a membrane potential of -40 mV and at pH 5.5 during a 30 s application (grey bar) of different sugar compounds (10 mM). Downward deflections indicate inward currents. (b) Current responses of BvPMT5a-expressing oocytes to the application of different sugar compounds (10 mM). The respective responses of each oocyte were normalized to the glucose-induced change in the inward currents of that oocyte. Data represents means ± SEM of 6 to 36 individual oocytes.

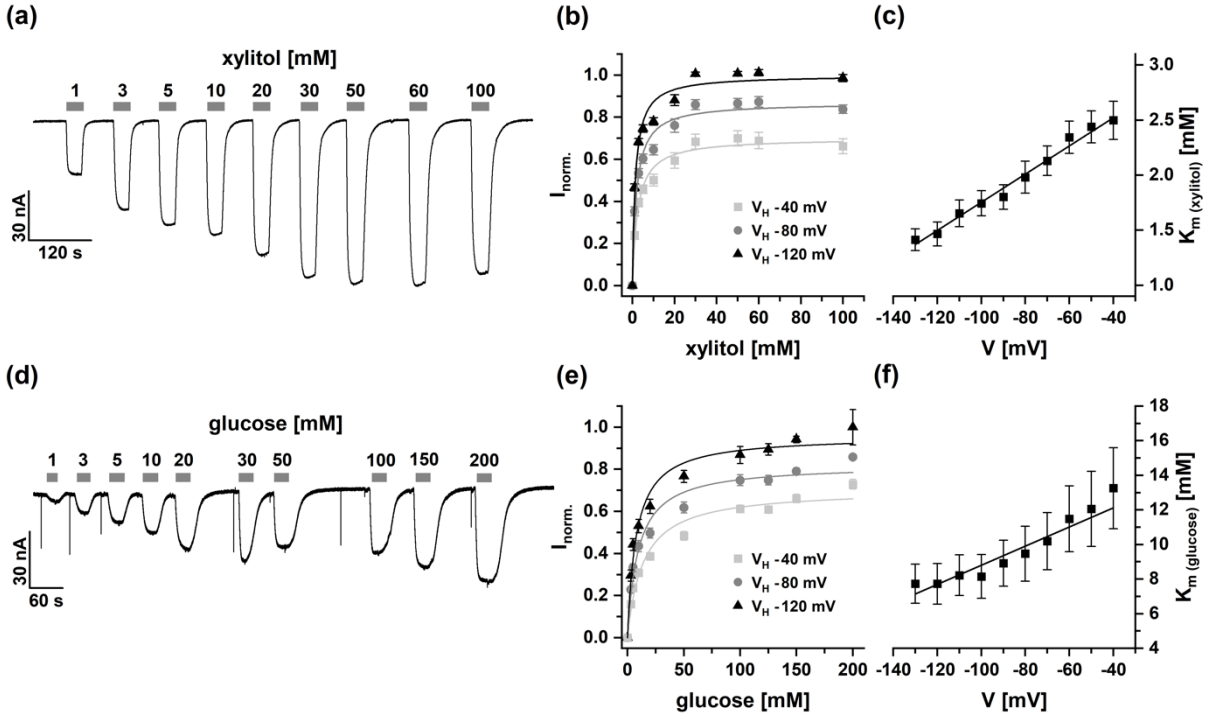

Fig. 3 Xylitol- and glucose-dose dependency of BvPMT5a. (a, d) Current responses of BvPMT5a-expressing oocytes to xylitol (a) or glucose (d) application at the indicated concentrations. The duration of the substrate administration is indicated by the grey bar above the current trace. Currents were recorded at a membrane voltage of -40 mV at pH 5.5. (b), (e), Xylitol- or- glucose-dependent currents plotted as a function of the substrate concentration. Currents were recorded at the membrane voltages as indicated and pH 5.5. Recorded currents were normalized to the maximum current recorded at a membrane voltage of -120 mV. The solid line gives the best fit of the data set with a Michaelis-Menten function. (c, f) Voltage dependency of the K_m values. K_m values derived from the best Michaelis-Menten-fits as shown in (b, e) were plotted against the respective membrane voltages. In (b, c) and (e, f) data represents means ± SEM of 9 and 10 individual oocytes, respectively.

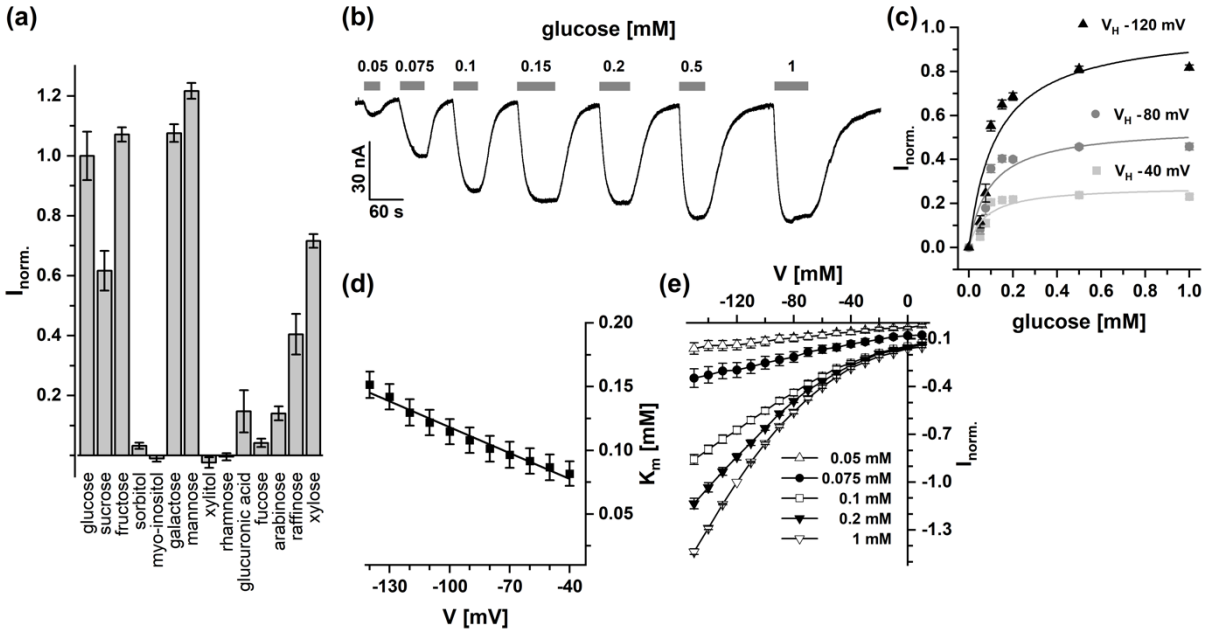

Fig. 4 Substrate specificity, glucose-dose and voltage dependency of BvSTP13. (a) Current responses of BvSTP13-expressing oocytes to the application of different sugar compounds (10 mM) recorded at a membrane voltage of -40 mV. The respective responses of each oocyte were normalized to the glucose-induced change in the inward currents of that oocyte. Data represents means ± SEM of 7 to 24 individual oocytes. (b) Representative current responses of BvSTP13-expressing oocytes to glucose application at the indicated concentrations. The duration of glucose administration is indicated by the grey bar above the current trace. Currents were recorded at a membrane voltage of -40 mV at pH 5.5. Noise peaks generated during the perfusion were dimmed offline. (c) Glucose-dependent BvSTP13-mediated currents plotted as a function of the substrate concentration. Currents were recorded at the membrane voltages indicated and pH 5.5. Recorded currents were normalized to the maximum current recorded at a membrane voltage of -120 mV. The solid line gives the best fit of the data set with a Michaelis-Menten function. (d) Voltage dependency of the K_m values. K_m values derived from the best Michaelis-Menten-fits as shown in C were plotted against the respective membrane voltages. (e) Current-voltage curves recorded at pH 5.5 under glucose treatment at indicated concentrations. Currents measured were normalized to the response to 1 mM glucose measured at -120 mV. In (a-e) all experiments were conducted at pH 5.5. In (c-e) data represents means ± SEM of 12 individual oocytes.

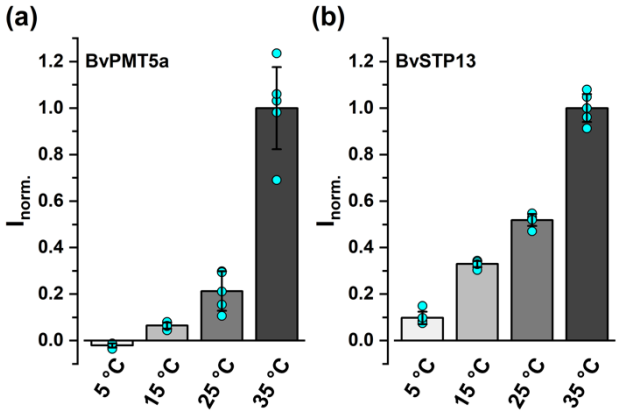

Fig. 5 Temperature dependency of BvPMT5a and BvSTP13. Current responses of BvPMT5a (a)- and BvSTP13 (b)-expressing oocytes to 50 or 0.5 mM glucose, respectively, measured at -140 mV and temperatures as indicated were normalized to those at 35 °C. A Q_{10} value of 3.97 ± 0.57 for BvPMT5a and 2.18 ± 0.64 for BvSTP13 (means ± SD, n = 5) was determined. Q_{10} values were calculated as mean factors between temperatures, which resulted in distinct currents in the range of 15 - 35 °C for BvPMT15 and 5 - 35 °C for BvSTP13 (mean ± SD of 5 individual oocytes). Turquoise circles indicate the individual data points.

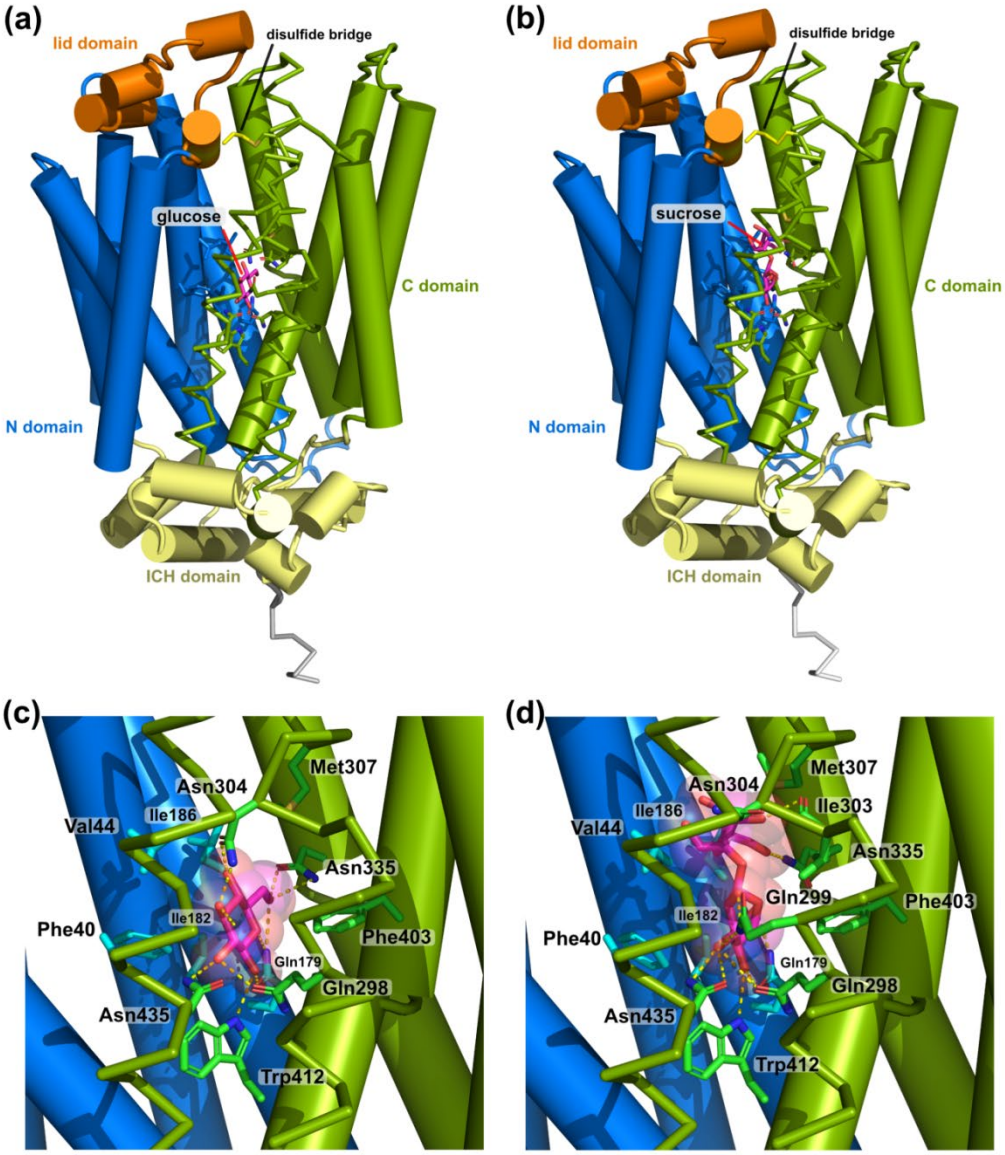

858

859 **Fig. 6** Comparison of a BvSTP13 model bound to glucose and sucrose. (a) A BvSTP13 model
860 with glucose bound in the saccharide binding site. (b) BvSTP13 3D model bound to sucrose.
861 The BvSTP13 model follows the color-coding scheme to indicate the different domains as
862 stated in Fig. S8. The saccharide moieties are shown as stick representation with their carbon
863 atoms colored in magenta and the oxygen atoms marked in red. (c) An enlargement of the
864 binding site in the interaction of BvSTP13 with glucose is shown. Residues in close proximity
865 (≤ 5 Å) are shown as sticks, hydrogen bonds between the glucose molecule and residues of
866 BvSTP13 are indicated by stippled lines colored in yellow. (d) The binding site of a BvSTP13
867 model interacting with sucrose is shown (magnification). The sucrose molecule was docked
868 into the saccharide binding site of our BvSTP13 homology model such that the glucose
869 moiety of the sucrose occupied the same position as the glucose molecule in the AtSTP10

structure. Energy minimization was performed, and a 10 ns MD trajectory was calculated with BvSTP13 placed in a bilayer membrane and the extra- and intracellular part surrounded by water. The model shows that the glucose moiety of the sucrose molecule can engage in similar hydrogen bonds as the glucose in the BvSTP13-glucose model. Furthermore, the fructose moiety of the sucrose molecule can form hydrogen bonds for instance with the carbonyl of Ile303 and with the carboxyamide group of Asn335.

Supporting Information

Fig. S1. Cellular loading of esculin in taproot cells.

Fig. S2. Sucrose-induced changes in H^+ fluxes and membrane depolarization of *Beta vulgaris* taproot cells.

Fig. S3. Phylogenetic tree of PMTs and STPs of *Arabidopsis thaliana* (At) and *Beta vulgaris* (Bt).

Fig. S4. Effect of low temperature on expression of *STP*- and *PMT*-like genes in *Beta vulgaris* taproots.

Fig. S5. pH and voltage dependency of BvPMT5a.

Fig. S6. Sucrose-dose dependency and voltage dependency of BvSTP13.

Fig. S7. pH and voltage dependency of BvSTP13.

Fig. S8. Comparison of the 3D homology model of BvSTP13 model and the crystal structure of AtSTP10.

Fig. S9. Structure guided alignment of sugar transporters.

Methods S1 Esculin uptake in Beta vulgaris taproot cells

904 **Methods S2** Gene expression analysis

905

906 **Supporting References**

907